Materials and Design 33 (2012) 115–120

Contents lists available at ScienceDirect

Materials and Design

journal homepage: www.elsevier.com/locate/matdes

Technical Report

Some studies on sintered cold deformed plain carbon alloy steels

A. Rajeshkannan [a,*], K.S. Pandey [b], S. Shanmugam [c], R. Narayanasamy [d], S. Narayan [a,1]

[a] Mechanical Engineering, School of Engineering and Physics, Faculty of Science, Technology & Environment, The University of the South Pacific, Laucala Campus, PO Box 1168, Suva, Fiji
[b] Department of Metallurgical and Materials Engineering, National Institute of Technology, Tiruchirappalli 620 015, Tamil Nadu, India
[c] Department of Mechanical Engineering, National Institute of Technology, Tiruchirappalli 620 015, Tamil Nadu, India
[d] Department of Production Engineering, National Institute of Technology, Tiruchirappalli 620 015, Tamil Nadu, India

ARTICLE INFO

Article history:
Received 2 June 2011
Accepted 8 July 2011
Available online 18 July 2011

ABSTRACT

Steel of Fe–0.8%C with and without addition of 1.0%Mo were considered for the present investigation. Experimental analysis was studied for attained density against induced strain parameter. Various stress parameters were determined and studied for its behaviour against strain. Instantaneous plastic Poisson's ratios of were computed and was compared with conventional. All these characteristics were extensively studied under the influence of composition as well as aspect ratios; however, friction condition and initial density of the preforms were kept constant.

1. Introduction

Powder metallurgy (P/M) has been used extensively to fabricate near net-shape parts for a wide variety of industries. One of the largest users of P/M net shape components is the automotive industries [1,2]. P/M techniques involve starting with clean metal powder with a desired microstructure and consolidating the powder aggregate into the final part geometry with the fewest number of processing steps, thus it offers inexpensive manufacturing. Several methods in P/M been evolved to produce parts, however, the process or route by which final shape achieved determines the property of these P/M parts. Most of the properties of P/M materials are strongly related to porosity as the pores act as stress concentration points results into crack initiation. Besides, their presences cause inhomogeneous stress distribution across the cross section of parts which lead to reduction of the effective load bearing area. Mechanical behaviour of sintered P/M alloys is significantly influenced by the inherent porosity, which can be removed to a great extend when the sintered alloys are subjected to cold or hot forging subsequent to sintering [3,4]. Deformation process on sintered parts leads to extensive plastic deformation results into improvement of density or reduction of porosity which subsequently encountered in enhancement of mechanical properties. Rajeshkannan and Sumesh [5] presented that the axial strain induced in P/M preforms result in creating subsequent lateral flow, however, a spherical pore will undergo flattening and simultaneous elongation in the direction normal to applied load. The shear stress present along with the normal pressure ensures that there is a relative motion between the opposite sides of the collapsing pores. Thus, mechanical rupturing of the oxide film is feasible, with the virgin material being exposed for bond formation across the collapsing pore surfaces. In case of cold working P/M material experience geometric strain hardening along with mechanical strain hardening due to the consequence of densification and deformation, respectively [6].

During the elastic deformation of fully dense material, Poisson's ratio remains constant and is a property of the material and during the plastic deformation of conventional materials, this ratio being 0.5 for all materials that conform to volume constancy [7]. However, in the plastic deformation of sintered P/M preforms, density changes occur resulting in Poisson's ratio remaining less than 0.5 and only approaching to 0.5 in the near vicinity of the theoretical density [8]. Kahlow [9] reported that increase in the volume of the voids decrease the relative critical pressure (the pressure just needed to close the voids) and vice versa. However, the closing and opening of voids occur with tri-axial compression and tension, respectively, with the absolute values of the relative critical pressure remaining the-same in each case. Whenever the relative critical pressure is exceeded, a void of given geometry begins to open faster in tension than it would close under tri-axial compression of the same magnitude [10]. The factors determining the geometry change of the pore are the pattern and the level of the plastic deformation [11]. Thus, it is obvious that the beginning and the continuation of pore closure can be accomplished at a comparatively lower pressure when the material is subjected to plastic deformation.

In frictionless compression tests for sintered P/M preforms, the deformation is expected to be uniform, showing no barreling of the cylindrical surface. However, reports on barreling in P/M cylindrical preforms under axial deformation are described elsewhere

* Corresponding author. Tel.: +679 3232695; fax: +679 3231538.
E-mail addresses: ananthanarayanan_r@usp.ac.fj (A. Rajeshkannan), pandey@nitt.edu (K.S. Pandey), shunt@nitt.edu (S. Shanmugam), narayan@nitt.edu (R. Narayanasamy), narayan_su@usp.ac.fj (S. Narayan).
[1] Tel.: +679 3232034; fax: +679 3231538.

0261-3069/$ - see front matter © 2011 Elsevier Ltd. All rights reserved.
doi:10.1016/j.matdes.2011.07.020

[12,13]. The decrease in aspect ratio along with an increase in friction at contact surfaces increases the curvature of the bulged surface. The non-uniform deformation in the presence of frictional forces results in the existence of secondary tensile stresses in the circumferential direction accompanying the axial compressive stresses [14]. Since the primary cause of the fracture in upsetting is tensile stresses, it is therefore essential to investigate fracture during the deformation processing of sintered powder materials with the help of axial upsetting tests.

The present investigation is aimed at evaluating the deformation behaviour of Fe–0.8%C and Fe–0.8%C–1.0%Mo sintered steel preforms during the cold upsetting test because of the industrial importance attached to the aforesaid material. An attempt has been made to investigate the influence of preform geometry and effect of 1.0%Mo in Fe–0.8%C during cold upsetting of constant initial fractional theoretical density (0.86) by using zinc stearate as a die surface-preform lubricant. Also, an attempt is made to establish the relationship between the fractional theoretical density, the Poisson's ratio and other parameters namely, the stress, strain and strain factor for with and without added 1.0%Mo in eutectoid steel preforms.

2. Experimental details

2.1. Materials

Atomized iron powder of −150 μm (particle size less than 150 μm size) was obtained from Sundaram Fasteners Limited, Hyderabad, India. Molybdenum of −37 μm and graphite of 2–3 μm was supplied by Metal Powder Company, Madurai, India and Ashburry Graphite Mills Inc., Ashburry Warren County, New Jersey, USA, respectively. Upon analysis, it was found to contain 99.7 and 99.8 percent purities, respectively, for the iron and molybdenum powder and the rest were insoluble impurities. The characteristics of the iron powder and its blend are given in Table 1. The apparent density, flow rate, compressibility and sieve analysis were performed using respective ASTM standards [15–17].

2.2. Blending and compacting

A powder mix corresponding to Fe–0.8%C and Fe–0.8%C–1.0%Mo steel were taken in a separate stainless steel pot with the powder mix to porcelain ball (10 –15 mm diameter) ratio of 1:1 by weight. The pot was very securely tightened and fixed on the pot mill to carry out the blending operation. The mill was operated for a period of 20 h to obtain a homogeneous powder blend. But, after an interval of 1 h, nearly 100 g of powder mix was taken out for the measurement of flow rate and apparent density (using ASTM standard [15]) and returned back to the pot as soon as the aforesaid measurements were carried out. Once the value obtained for flow rate and apparent density became quite consistent, the blending operation was terminated. Thus, the most ideal time for Fe–0.8%C and Fe–0.8%C–1.0%Mo were found to be 19–20 h. Green compacts of 27.5 mm diameter and 14 & 28 mm of length were prepared on a 1.0 MN capacity hydraulic press using suitable die, punch and bottom insert (using ASTM standard [18]). The initial

Table 1
Characterization of iron powder and powder blends.

Si. No.	Property	Iron	Fe–0.8%C blend	Fe–0.8%C–1.0%Mo blend
1.	Apparent density (g/cc)	2.96	2.87	2.86
2.	Flow rate, (s/50 g) by hall flow meter	28.0	26.8	25.5
3.	Compressibility (g/cc) at pressure of 430 ± 10 MPa	6.55	6.50	6.50
4.	Sieve size analysis of iron powder			

Sieve size (μm)	150	+126	+106	+90	+75	+63	+53	+45	+37	−37
wt% ret.	10.14	21.90	9.46	2.02	20.10	12.10	11.10	5.70	0.31	7.00

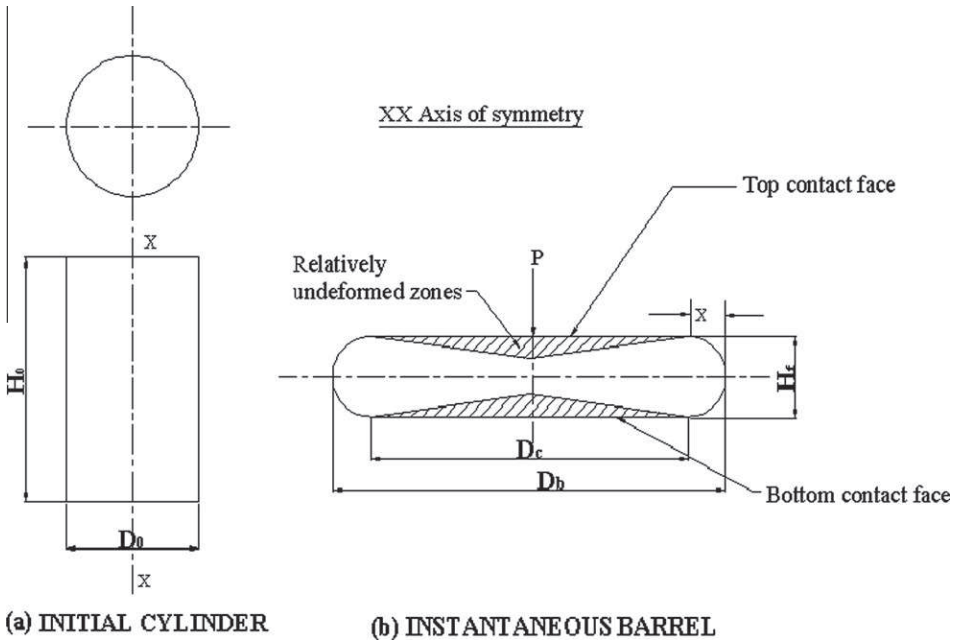

Fig. 1. Schematic representation of upset forging test specimen before and after deformation.

preform densities were maintained in the range of 86 ± 1% of theoretical by employing pressure in the range of 430 ± 10 MPa.

2.3. Sintering

Indigenously developed [8] ceramic coating was applied on the entire surface of all the green compacts to protect them against oxidation during the sintering and the cooling schedules. After the first coating was dried for a period of 12 h under the ambient conditions, the compacts were recoated in the direction 90° to the previous one. The second coating was dried for a further period of 12 h under the aforesaid conditions. Further, these ceramic-coated compacts were dried at 700 °C for a period of 30 min in an alumina boat placed inside the electric muffle furnace. After the drying sequence was completed, the furnace temperature was raised to 1150° ± 10 °C. At this temperature, the compacts were sintered for 90 min. As soon as the sintering schedule was completed, the sintered preforms were cooled inside the furnace itself at room temperature.

2.4. Cold deformation

The sintered preforms were machined to yield initial aspect ratio of 0.40 and 0.75, respectively, and measurements such as initial height, diameter and densities were carried out before and after each of deformations, the latter being carried out between two flat dies heat treated to Rc 52–55 and tempered to Rc 46–48. The die surfaces were mirror polished. During the cold compression test, zinc stearate lubricant was used at both of the die contact surfaces, which ensured the minimum friction, resulting in quite homogeneous deformation. In general, each compact was subjected to compressive loading in steps of 0.04 MN until fine cracks appeared on its free surface. Fig. 1 shows the schematic diagram of the upsetting process before and after deformation. Immediately after the completion of each step of loading, the height, the contact diameters (at the top and bottom), the bulged diameter and the density measurements being carried out following the procedures, described elsewhere [19,20]. Experimental measurements were also used to calculate the various parameters such as, the stresses, the strain and the Poisson's ratio.

3. Theoretical analysis

The present investigation is based on the analytical determination of the deformed density, strains, stresses, and the plastic Poisson's ratio. In the present investigation, the material under consideration is porous. As explained elsewhere [21], the expression for the bulging of a cylindrical preform of fully dense material can be written as follows, provided that the bulging contour assumes the form of a circular arc:

$$\frac{\pi}{4}D_0^2 h_0 = \frac{\pi}{12}(2D_b^2 + D_c^2)h_f \tag{1}$$

Eq. (1) is based on the volume-constancy principle. However, the same is not true for porous preform upsetting; instead the mass-constancy principle is employed before and after deformation. As a result of it, Eq. (1) converts to:

$$\frac{\pi}{4}D_0^2 h_0\left(\frac{\rho_0}{\rho_{th}}\right) = \frac{\pi}{12}(2D_b^2 + D_c^2)h_f\left(\frac{\rho_f}{\rho_{th}}\right) \tag{2}$$

where D_0 is the initial diameter (cm); h_0 is the initial height of the cylindrical preform (cm); ρ_0 is the initial preform density of the cylinder (g/cc); D_b is the bulged diameter (cm); D_c is the contact diameter (cm); h_f is the height of the preform during deformation; ρ_f is the density of the preform after deformation, (g/cc); and ρ_{th} is the theoretical density of the fully dense material (g/cc).

Eq. (2) can be rearranged as below:

$$\left(\frac{\rho_f}{\rho_{th}}\right) = \left(\frac{\rho_0}{\rho_{th}}\right)\left(\frac{h_0}{h_f}\right)\left(\frac{3D_0^2}{2D_b^2 + D_c^2}\right) \tag{3}$$

Taking natural logarithms on both sides of Eq. (3), the following expression is obtained:

$$\ln\left(\frac{\rho_f}{\rho_{th}}\right) = \ln\left(\frac{\rho_0}{\rho_{th}}\right) + \ln\left(\frac{h_0}{h_f}\right) - \ln\left(\frac{2D_b^2 + D_c^2}{3D_0^2}\right) \tag{4}$$

However, Eq. (4) can be further simplified to:

$$\left(\frac{\rho_f}{\rho_{th}}\right) = \left(\frac{\rho_0}{\rho_{th}}\right)e^{\varepsilon_z - \varepsilon_\theta} \tag{5}$$

where $\varepsilon_z = \ln(h_0/h_f)$ and $\varepsilon_\theta = \ln((2D_b^2 + D_c^2)/3D_0^2)$

Since the ratio (ρ_0/ρ_{th}) is taken as constant, Eq. (5) shows an exponential relationship between the density ratio (ρ_f/ρ_{th}) and the difference between the two true strain ε_z and ε_θ. Now defining a new or instantaneous Poisson's ratio (ψ) based on the contact and bulged diameter as

$$\psi = \frac{\varepsilon_\theta}{2\varepsilon_z} \tag{6}$$

which enables Eq. (6) to be written as

$$\psi = \ln\left(\frac{2D_b^2 + D_c^2}{3D_0^2}\right) \Big/ \ln\left(\frac{h_0^2}{h_f^2}\right) \tag{7}$$

From reports published elsewhere [22], the associated flow characteristics for porous materials under plane strain conditions (here σ_y is taken to be zero) can be expressed as follows:

$$d\varepsilon_z = d\lambda(\sigma_z - \nu\sigma_\theta) \tag{8}$$

$$d\varepsilon_\theta = d\lambda(\sigma_\theta - \nu\sigma_z) \tag{9}$$

where $d\varepsilon_z$ is the plastic strain increment in the axial direction; $d\varepsilon_\theta$ is the plastic strain increment in the hoop direction; $d\lambda$ is the constant; σ_z is the true stress in the axial direction; σ_θ is the true stress in hoop direction; ν is the conventional Poisson's ratio and it is expressed as follows:

$$\nu = \left(\frac{\ln(D_c/D_0)}{\ln(h_0/h_f)}\right) \tag{10}$$

Now dividing Eq. (9) by Eq. (8), the following expression can be obtained

$$\frac{d\varepsilon_\theta}{d\varepsilon_z} = \frac{(\sigma_\theta - \nu\sigma_z)}{(\sigma_z - \nu\sigma_\theta)} \tag{11}$$

Eq. (11) can be further simplified as follows:

$$\frac{\sigma_\theta}{\sigma_z} = \frac{\alpha + \nu}{1 + \alpha\nu} \tag{12}$$

where $\alpha = (d\varepsilon_\theta/d\varepsilon_z)$; Eq. (12) can be further written as

$$\sigma_\theta = \left(\frac{\alpha + \nu}{1 + \alpha\nu}\right)\sigma_z \tag{13}$$

Now substituting the value for the true axial stress, σ_z, the true hoop stress, σ_θ, can be calculated, where σ_z = load/contact surface area.

Further, using the values of σ_z and σ_θ, the hydrostatic stress (σ_m) can be calculated using the relationship given below:

$$\sigma_m = \left(\frac{\sigma_z + \sigma_\theta}{3}\right) \tag{14}$$

4. Results and discussion

Stress–strain analysis is considered to be the fundamental when discussing the mechanical behaviour of any wrought or P/M materials subjected to any form of external loading condition [5]. Stress determines the internal resistance of a material against the external disturbance on a particular area of cross section exposed to deformation while strain normally deals with the deformation of the body. Fig. 2 shows the effect of with and without addition of 1.0% molybdenum in eutectoid steel on the characteristic features of the axial stress, σ_z, as a function of the axial strain, ε_z, for two different aspect ratios. These plots are similar in nature irrespective of composition and aspect ratio. It is observed that effect of molybdenum in Fe–0.8%C is quite dominant in the later stages than in the initial stages of deformation, this being true invariable for all aspect ratios. It shows that the true axial stress increases rapidly as the true height strain is increased, followed by a gradual increase in true axial stress with further increase in true height strain. Further, it is found that a preform with 1.0% molybdenum addition exhibits improved load bearing capacity compared with the plain eutectoid steel preform, subject to the condition that the initial preform density and deforming media taken is kept constant. In addition, it is important to observe that the effect of aspect ratio is distinct when molybdenum is added in eutectoid steel and the same is not true in Fe–0.8%C P/M steel. Further, strain to fracture values is enhanced for plain eutectoid steel preform compared to a preform with 1.0% molybdenum addition.

It is well known [8,23–25] that densification is continuously enhanced during the deformation process; therefore, densification is a function of induced strain. In this view Fig. 3 has been drawn to establish the relationship between the fractional theoretical density (ρ_f/ρ_{th}) of the deforming preform and the value of $e^{\varepsilon_z-\varepsilon_\theta}$ in accordance with the theoretically derived relationship (Eq. (5)) for sintered P/M preforms during cold upsetting deformation. These plots show the existence of power law relationship between the fractional theoretical density and $e^{\varepsilon_z-\varepsilon_\theta}$ with a constant slope of 0.90, this being so irrespective of the aspect ratio and the compositions taken. Further, it is important to note at the start of deformation there is a drastic increment of attained density (very less in magnitude), representing a mechanism common for both aspect ratios as well as compositions. This is due to high resistance against deformation, however, this can be neglected for all practical purpose. Similarly, at the final stage almost all the points are accumulated and overlapped irrespective of aspect ratios and compositions, which shows no definite mechanism, this is due to that the material gets work hardened and it exhibits high resistance to deformation as a consequence it attains very little densification. In general, increase in the value of $e^{\varepsilon_z-\varepsilon_\theta}$ show an increasing trend in the values of ρ_f/ρ_{th} for all the aspect ratio and compositions. Further, it is found that a lower aspect ratio (0.40) exhibits improved densification compared to that for higher aspect ratio (0.75) preforms irrespective of with and without addition of molybdenum in eutectoid steel. Figs. 2 and 3 are essential in designing of preform geometry as well as dies for cold upset forging.

The stresses, namely, the axial (σ_z) the hoop (σ_θ) and the hydrostatic (σ_m) increase with the increasing level of axial strains (ε_z), as shown in Fig. 4. The hoop stress is tensile in nature because during compressive loading the bulge diameter expands. However, for any deformation level, the increase in hoop stress due to loading is very low compared to that of the axial stress. However, the value of the hydrostatic stress is much less than the other stresses, namely, axial and hoop stress and it is also compressive in nature.

During cold upsetting of P/M materials, material flows into the pores or voids and consequently there is a decrease in bulk volume. Further, for a given height strain, the diameter strain of P/M material will be lesser in magnitude than for a fully dense material [23,26]. Poisson's ratio is defined as ratio between the lateral strain and axial strain and is one of the most important dimensionless parameter which is effectively used in the forming of powder metallurgy parts. Fig. 5 has been drawn to exhibit the relationship between the value of Poisson's ratio (calculated based only on contact diameter, Eq. (10)) and the fractional theoretical density achieved during cold upset forming (axial deformation). These plots being drawn for two initial aspect ratios and two different compositions, namely, Fe–0.8%C and Fe–0.8%C–1.0%Mo. The characteristic features of these curves can be classified into three distinct categories. Category I describes a rapid rise in the values of Poisson's ratio with little densification, which means that the material offers

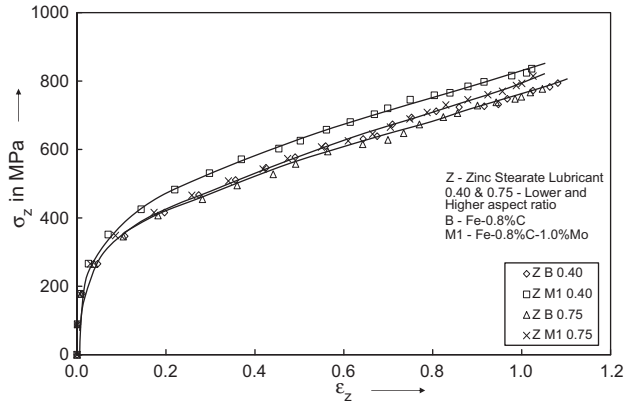

Fig. 2. The relationship between σ_z and ε_z.

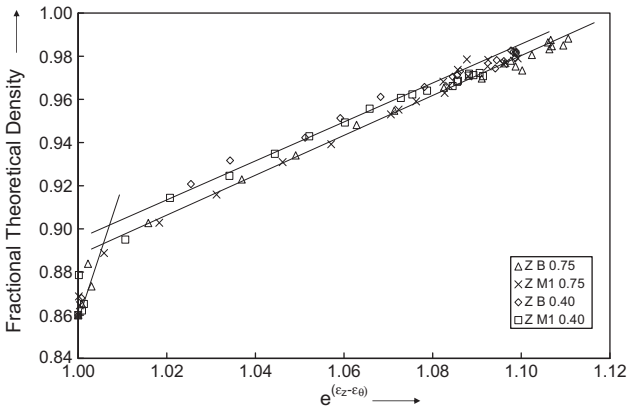

Fig. 3. The relationship between fractional theoretical density and $e^{\varepsilon_z-\varepsilon_\theta}$.

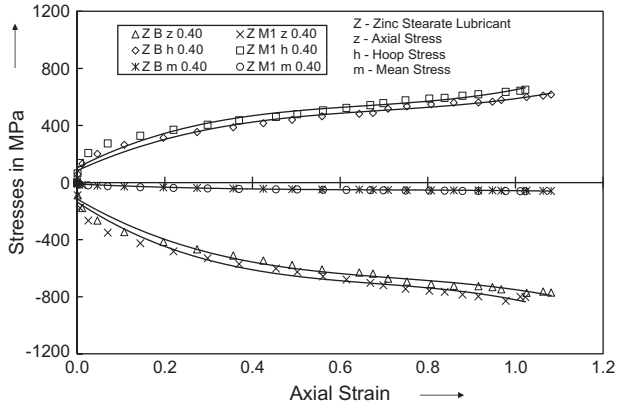

Fig. 4. The relationship between various stresses and axial strain for a given aspect ratio of 0.40.

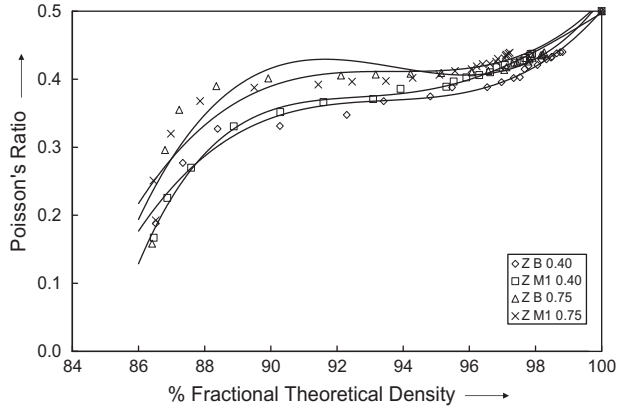

Fig. 5. The relationship between Poisson's ratio and percentage fractional theoretical density.

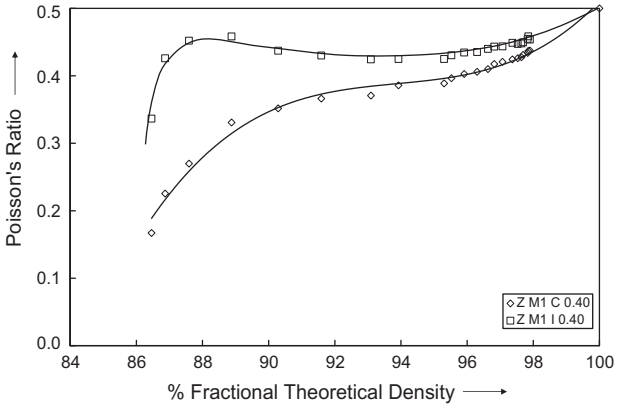

Fig. 6b. Variation of Poisson's ratio and percentage fractional theoretical density for Fe–0.8%C–1.0%Mo steel preforms of 0.40 aspect ratio.

initial resistance to deformation, as a consequence of which the preform undergoes more of a lateral deformation than that of a height strain (both being negligibly small). Category II is treated as a steady–state condition, where most of the densification occurs with a small increase in Poisson's ratio. During this stage, densification occurs mostly in the lateral and axial direction, due to the elimination of pores. Category III involves the stage where a rapid increase in Poisson's ratio occurred without much enhancement in the density values in the deforming preforms. In this region, the lateral spread is greater compared to the height strains. However, the tendency to approach a limiting value of 0.5 is seen, which is theoretically feasible value of Poisson's ratio and is in good agreement with Narayan et al. [27].

Fig. 6a and b shows the variation of Poisson's ratio calculated: (i) Based only on the contact diameter, conventional Eq. (10); and (ii) Based on both the contact and the bulged diameters, instantaneous Eq. (6); with respect to the fractional theoretical density, for the given aspect ratio of 0.40. It is found that for any given composition and the fractional theoretical density values, the values of instantaneous Poisson's ratio obtained based on both contact and bulged diameter is greater than that obtained based on only contact diameter. The difference between these two values of Poisson's ratio is considerably more substantial when the fractional theoretical density values are less. However, as the fractional theoretical density value approaches the theoretical value, the above difference become negligible.

Cold working is one of the best methods employed to promote strength in P/M materials, however, the important factor remains is the pore closure or density attained [27]. The strength and other

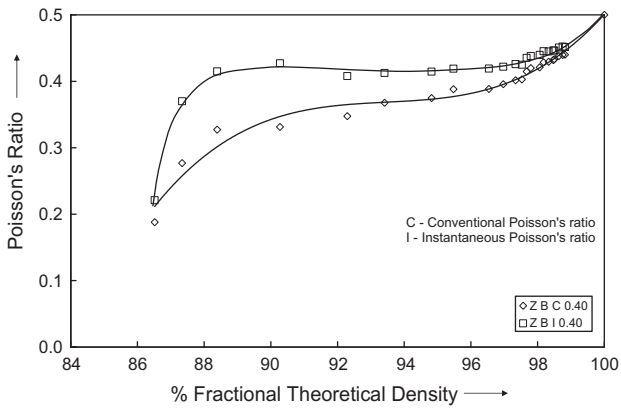

Fig. 6a. Variation of Poisson's ratio and percentage fractional theoretical density for Fe–0.8%C steel preforms of 0.40 aspect ratio.

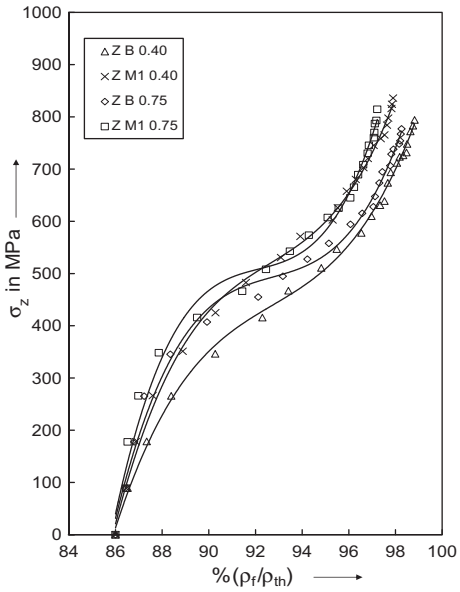

Fig. 7. The relationship between σ_z and $\%(\rho_f/\rho_{th})$.

mechanical properties are very much dependent on the maximum density attained by the P/M material and the mode by which this density is achieved [28]. In broad prospect, strength can be expressed as the resistance against deformation up to its fracture. Therefore, the strength can also be the function of attained density. Thus, Fig. 7 has been drawn to demonstrate the relationship between the axial stress, σ_z, and the percentage theoretical density, $\%(\rho_f/\rho_{th})$, this figure also showing the effect of aspect ratio and composition on the aforesaid relationship. In general, the axial stress has the tendency to increase rapidly during the initial stage of densification, thereafter continuing to increase, but at a lesser rate, as the densification increases, the increase in axial stress being associated with the combined effects of densification on the geometric and general work-hardening. However, the preforms of 1.0%Mo added eutectoid P/M steel as well as preform of higher aspect ratio (0.75) irrespective of composition, shown more stress than its respective counter part preforms.

5. Conclusions

The basic conclusions that can be drawn from the present investigation are as follows:

1. A power law relationship between the fractional theoretical density (ρ_f/ρ_{th}) and $e^{\varepsilon_z-\varepsilon_\theta}$ has been established. This remained valid for plain and 1.0%Mo added eutectoid steel and for all the aspect ratios.
2. The Poisson's ratio value determined for conventional and instantaneous found to be differing, however, its characteristic nature is similar, besides both are having tendency to approach a limiting value of 0.5 in the near vicinity of the theoretical density.
3. The stresses, namely, the axial (σ_z), the hoop (σ_θ) and the hydrostatic (σ_m) can be calculated and are found to have an increasing trend with enhanced level of deformation. However, the applied stress increased rapidly in the early stage of deformation, and then continues to increase but at a lesser rate, as the deformation continues. The inclusion of 1.0%Mo in eutectoid steel improves the load bearing capacity irrespective of aspect ratios. Similarly, increase of aspect ratio increases the level of stresses for a given fractional theoretical density irrespective of composition.
4. The above plots are essential in designing of forming operations for Fe–0.8%C with and without addition of 1.0%Mo.

References

[1] Mac Donald BJ, Hashmi MSJ. Near-net-shape manufacture of engineering components using bulge-forming processes: a review. J Mater Process Technol 2002;120:341–7.

[2] Narayanasamy R, Senthilkumar V, Pandey KS. Some features on hot forging of powder metallurgy sintered high strength 4%titanium carbide composite steel preforms under different stress state conditions. Mater Des 2008;29:1380–400.

[3] Shanmugasundaram D, Chandramouli R, Kandavel TK. Cold and hot deformation and densification studies on sintered Fe–C–Cr–Ni low alloy P/M steels. Int J Adv Manuf Technol 2009;41:8–15.

[4] Kandavel TK, Chandramouli R, Ravichandran M. Experimental study on the plastic deformation and densification characteristics of some sintered and heat treated low alloy powder metallurgy steels. Mater Des 2010;31:485–92.

[5] Rajeshkannan A, Narayan S. Strain hardening behaviour in sintered Fe–0.8%C–1.0%Si–0.8%Cu powder metallurgy preform during cold upsetting. J Eng Manuf 2009;223:1567–74.

[6] Rajeshkannan A, Pandey KS, Shanmugam S, Narayanasamy R. Deformation behaviour of sintered high carbon alloy P/M steel in powder preform forging. Mater Des 2008;29:1862–7.

[7] Hoffmann H, Vogl C. Determination of True stress–strain–curves and normal anisotropy in tensile tests with optical strain measurement. CIRP Annals Manuf Technol 2007;52:217–20.

[8] Rajeshkannan A, Pandey KS, Shanmugam S. Some investigation on the cold deformation behaviour of sintered iron–0.8% carbon alloy powder preforms. J Mater Process Technol 2008;203:542–7.

[9] Kahlow KJ. Void behaviour as influenced by pressure and plastic deformation. Institute for Metal Forming Report: Lehigh University; 1971. p. 10–6.

[10] Gaiger HL, Lawley A. Changes during the densification of P/M preforms. Int J Powder Metall Powder Technol 1974;10:21–31.

[11] Mamalis AG, Petrossian GL, Manolakos DE. The effect of porosity and microdefects on plastically deformed porous materials. J Mater Process Technol 1999;96:117–23.

[12] Rajeshkannan A, Pandey KS, Shanmugam S, Narayanasamy R. Some studies on barreling of powder preforms during cold upsetting. J Mech Behav Mater 2006;17:415–30.

[13] Baskaran K, Narayanasamy R. Some aspects of barreling in elliptical shaped billets of aluminium during cold upset forging with lubricant. Mater Des 2008;29:638–61.

[14] Kim HS, Won CW, Chun BS. Plastic deformation of porous metal with an initial inhomogeneous density distribution. J Mater Process Technol 1998;74:213–7.

[15] B212-09. Standard test method for apparent density of free-flowing metal powders using the hall flowmeter funnel. ASME standards; 2010.

[16] B331-95. Standard test method for compressibility of metal powders in uniaxial compaction. ASME standards; 2002.

[17] B214-07. Standard test method for sieve analysis of metal powders. ASME standards; 2007.

[18] B925-08. Standard practices for production and preparation of powder metallurgy test specimens. ASME standards; 2008.

[19] B962-08. Standard test methods for density of compacted or sintered powder metallurgy products using Archimedes' principle. ASME standards; 2009.

[20] Moyer KH. Measuring density of powder metallurgy materials with improved precision. Int J Powder Metall Powder Technol 1979;15:33–42.

[21] Narayanasamy R, Pandey KS. Some aspects of barreling of porous solid cylinders under axial compression. Int J Powder Metall Sci Technol 1990;1:24–34.

[22] El Wakil SD. On the work hardening of sintered porous materials. In: Proceedings of 12th North American manufacturing research conference; 1984. p. 86.

[23] Narayanasamy R, Selvakumar N. Deformation behaviour of cold upset forming of sintered Al–Fe composite preforms. J Eng Mater Technol 2005;127:251–6.

[24] Rajeshkannan A, Pandey KS, Shanmugam S, Narayanasamy R. Sintered Fe–0.8%C–1.0%Si–0.4%Cu P/M preform behaviour during cold upsetting. J Iron Steel Res Int 2008;15:92–7.

[25] Narayanasamy R, Ramesh T, Pandey KS. Some aspects on workability of aluminium–iron powder metallurgy composite during cold upsetting. Mater Sci Eng A 2005;391:418–26.

[26] Narayanasamy R, Pandey KS. A study on the barreling of sintered iron preforms during hot upset forging. J Mater Process Technol 2000;100:87–94.

[27] Narayan S, Rajeshkannan A. Densification behaviour in forming of sintered iron–0.35% carbon powder metallurgy preform during cold upsetting. Mater Des 2011;32:1006–13.

[28] Vamsikrishna B, Venugopal P, Prasad RK. Analysis of deformation during simultaneous plastic deformation of dissimilar powder metallurgical preforms. Powder Technol 2004;146:137–46.